Three-dimensional analysis of post-Golgi carrier exocytosis in epithelial cells

Geri Kreitzer*#, Jan Schmoranzer‡§, Seng Hui Low¶, Xin Li¶, Yunbo Gan*, Thomas Weimbs¶, Sanford M Simon‡ and Enrique Rodriguez-Boulan*†

*Margaret M. Dyson Vision Research Institute, Weill Medical College of Cornell University, New York, NY 10021, USA
†Department of Cell Biology, Weill Medical College of Cornell University, New York, NY 10021, USA
‡Laboratory of Cellular Biophysics, Rockefeller University, New York, NY 10021, USA
§Department of Biology, Chemistry, Pharmacology, Free University, Berlin 14195, Germany
¶Department of Cell Biology, Lerner Research Institute and the Glickman Urological Institute, The Cleveland Clinic, Cleveland, OH 44195, USA
e-mail: #ggurlan@med.cornell.edu or **boulan@med.cornell.edu

Published online: 27 January 2003; DOI: 10.1038/ncb917

Targeted delivery of proteins to distinct plasma membrane domains is critical to the development and maintenance of polarity in epithelial cells. We used confocal and time-lapse total internal reflection fluorescence microscopy (TIR-FM) to study changes in localization and exocytic sites of post-Golgi transport intermediates (PGTIs) carrying GFP-tagged apical or basolateral membrane proteins during epithelial polarization. In non-polarized Madin Darby Canine Kidney (MDCK) cells, apical and basolateral PGTIs were present throughout the cytoplasm and were observed to fuse with the basal domain of the plasma membrane. During polarization, apical and basolateral PGTIs were restricted to different regions of the cytoplasm and their fusion with the basal membrane was completely abrogated. Quantitative analysis suggested that basolateral, but not apical, PGTIs fused with the lateral membrane in polarized cells, correlating with the restricted localization of Syntaxins 4 and 3 to lateral and apical membrane domains, respectively. Microtubule disruption induced Syntaxin 3 depolarization and fusion of apical PGTIs with the basal membrane, but affected neither the lateral localization of Syntaxin 4 or Sec6, nor promoted fusion of basolateral PGTIs with the basal membrane.

Epithelial cells perform polarized transport and secretory functions that are essential for survival of the organism. To perform these vectorial functions, epithelial cells segregate their plasma membrane proteins into apical and basolateral domains, separated by tight junctions. Apical and basolateral membrane proteins are synthesized in the endoplasmic reticulum, transferred to the Golgi apparatus and segregated into different PGTIs for export to the cell surface[1–3]. Segregation is thought to occur in the *trans*-Golgi network (TGN) and is mediated by sorting signals embedded within the protein structure. Apical sorting signals include N- and O-linked glycans in the ectodomain, glycosyl phosphatidylinositol and transmembrane anchors, and amino-acid stretches in the cytoplasmic domain[4,5]. In contrast, basolateral sorting signals usually comprise amino acid stretches in the cytoplasmic domain that typically include tyrosine, dileucine and monoleucine motifs, as well as clusters of acidic amino acids[6,7]. Apical or basolateral membrane proteins can exit the Golgi in vesicular or tubular PGTIs[3,8,9]. The formation of PGTIs depends on the direct or indirect interaction of sorting signals with cytoplasmic adaptors and coat proteins[10–13]. Adaptors can also mediate binding of cargo to specific microtubule motors[14–16], which can modulate the transport and/or budding of Golgi-derived vesicles, as well as the emergence of tubular PGTIs[9].

Work in the past two decades has suggested that microtubules are important in establishing epithelial polarity, although exactly how they contribute to this process is still unknown. During epithelial polarization, microtubules re-organize from centrosomally nucleated, radial arrays into longitudinal bundles (minus-ends towards the apical surface) oriented in parallel with the lateral membrane, and into arrays of mixed polarity underlying the apical pole and overlying the basal membrane[17,18]. This microtubule reorganization is accompanied by relocation of the Golgi complex to the apical region of the cytoplasm[17,19]. Time-lapse studies in fibroblasts and sub-confluent epithelial cells have shown that vesicular and tubular PGTIs move through the cytoplasm along microtubules for delivery to the plasma membrane[3,8,20]. Injection of kinesin antibodies completely inhibits post-Golgi transport, indicating that microtubules are essential for post-Golgi trafficking under physiological conditions[9]. In polarized epithelial cells, biochemical assays have shown that disruption of microtubules slows the delivery of apical membrane proteins and often results in their mis-targeting to the basolateral surface[18,19,21–27]. In contrast, disruption of microtubules does not significantly affect delivery of basolateral membrane proteins[22,24,28], but does induce apical exocytosis of proteins normally secreted into the basolateral medium[29,30]. Although the effects of microtubule disruption on apical and basolateral protein targeting have been well characterized, it is unclear whether and how microtubules exert selective control over the intracellular distribution of PGTIs, as well as over their fusion with specific domains of the plasma membrane.

A key event in epithelial polarization is the establishment of polarized transport routes to apical and basolateral regions of the plasma membrane. The asymmetric distribution of docking and fusion machinery for PGTIs is probably involved in regulating polarized exocytosis in epithelial cells. Basolateral exocytosis seems to depend on an evolutionarily conserved 'tethering' complex known as the exocyst. In polarized MDCK cells, the exocyst localizes to the lateral membrane near the tight junction[31]. Antibodies against the exocyst components Sec6 and Sec8 block basolateral

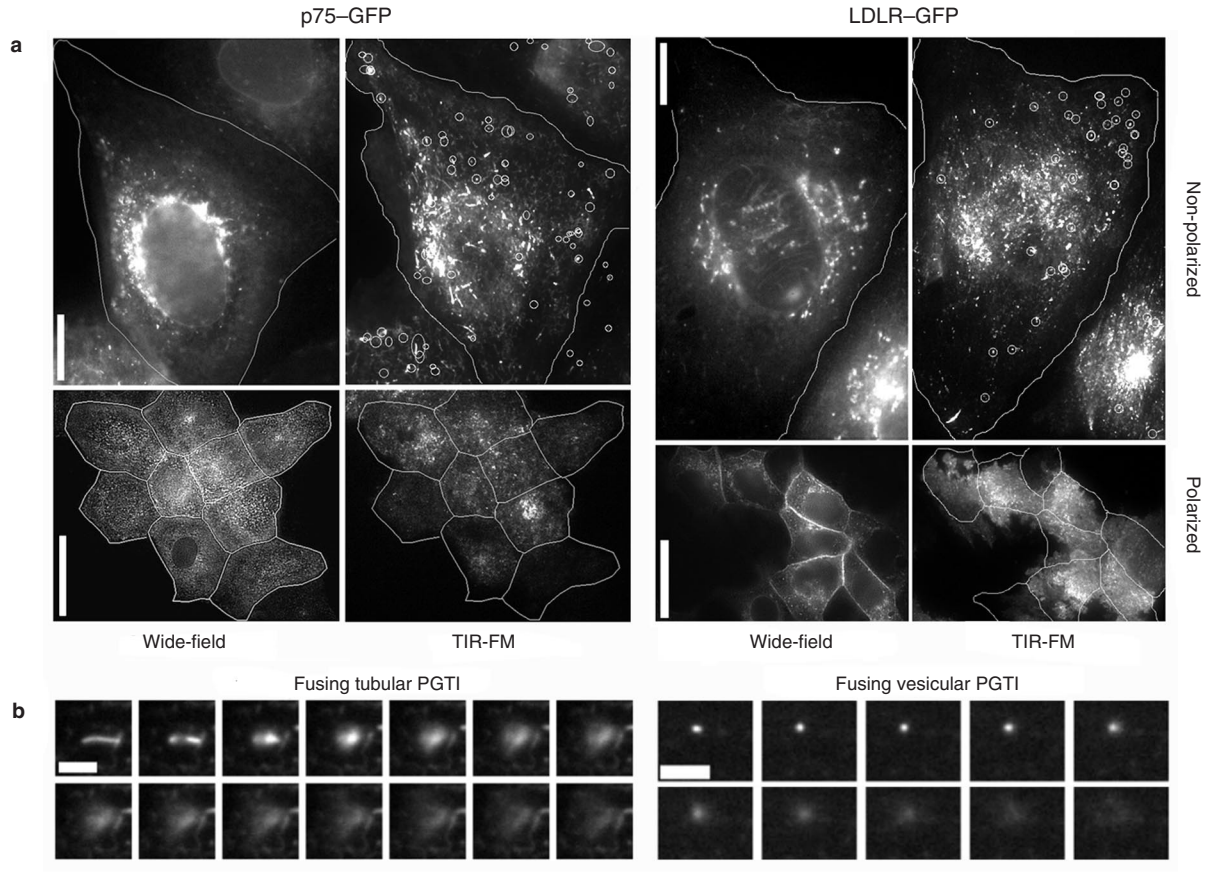

Figure 1 **Fusion of PGTIs with the basal membrane in MDCK cells.** Fusion of post-Golgi carriers with the basal plasma membrane was monitored by TIR-FM after release from a Golgi temperature block. 500-frame time-lapse sequences were acquired at 222-ms intervals, unless otherwise stated. **a**, Wide-field images of non-polarized cells show the total intracellular distribution of GFP-tagged membrane proteins just after release from the Golgi temperature block. TIR-FM images show time-lapse overlays (every 20 frames) from recordings made in cells expressing p75–GFP (21 min after release of the Golgi block; Supplementary Information, Movie 1) or LDLR–GFP (19 min after release of the Golgi block. Positions of fusion events mapped in Supplementary Information Movie 1 are circled in TIR-FM panels. In polarized cells, PGTIs containing p75–GFP or LDLR–GFP did not fuse with the basal membrane in polarized cells at any time after release of the Golgi block. Corresponding wide-field images of polarized cells show that although no fusion events were detected by TIR-FM, p75–GFP and LDLR–GFP emptied from the Golgi and localized to the apical and basolateral plasma membranes, respectively. **b**, Selected sequential frames from TIR-FM recordings showing examples of tubular or vesicular PGTIs fusing with the membrane are shown. Scale bars represent 15 μm in **a** and 2 μm in **b**. Accompanying movies can be found at http://www.boulan-lab.acomhosting.com.

transport[31], and overexpression of another exocyst component, Sec10, results in enhanced basolateral transport[32]. Components of the plasma membrane fusion machinery, the t-SNAREs Syntaxin 3 and 4, localize to apical and basolateral plasma membranes, respectively, in polarized MDCK cells[33]. In semi-intact MDCK cell transport assays, addition of α-SNAP antibodies or cleavage of the t-SNARE, SNAP23, with botulinum E toxin reduced surface delivery of apical and basolateral markers, whereas anti-Syntaxin 3 antibodies selectively inhibited apical transport[34,35]. In intact cells, overexpression of Syntaxin 3 results in decreased apical transport and a twofold accumulation of vesicles under the apical plasma membrane[34]. These data suggest that SNARE-mediated fusion events are essential to polarized exocytosis.

In this study, we used confocal microscopy and TIR-FM to analyse the three-dimensional distribution of apical and basolateral PGTIs, and to localize their sites of exocytosis in non-polarized and polarized MDCK cells. Additionally, we tested whether microtubules modulate the distribution of tethering or fusion complexes involved in generating polarized transport routes to the cell surface. Our results demonstrate that both apical and basolateral PGTIs fuse with the basal plasma membrane in non-polarized MDCK cells. After polarization, apical and basolateral PGTIs become spatially segregated in different regions of the apical cytoplasm; basolateral PGTIs were observed primarily in the most apical two thirds of the cytoplasm, whereas apical PGTIs were restricted to the top ~4 μm of the cytoplasm. In polarized cells, neither apical nor basolateral PGTIs fused with the basal membrane. Instead, fusion of basolateral PGTIs was concentrated in upper regions of the lateral membrane. Apical PGTIs were not observed fusing with either the basal or lateral membrane in polarized cells, suggesting that these carriers fused directly with the apical membrane. In contrast, disruption of microtubules with nocodazole promoted fusion of apical PGTIs with the basal membrane and depolarization of apical Syntaxin 3. We show that micro-injection of a function-blocking antibody against Syntaxin 3 inhibits delivery of an apical marker in polarized, untreated MDCK cells, as well as its fusion with the basal membrane when microtubules were depolymerized. Our results implicate microtubules in maintaining the apical distribution of Syntaxin 3, and thus in prohibiting fusion of apical PGTIs with the basolateral membrane. This study represents the first live-cell analysis of the three-dimensional distribution of post-Golgi transport intermediates and their fusion with restricted domains of the

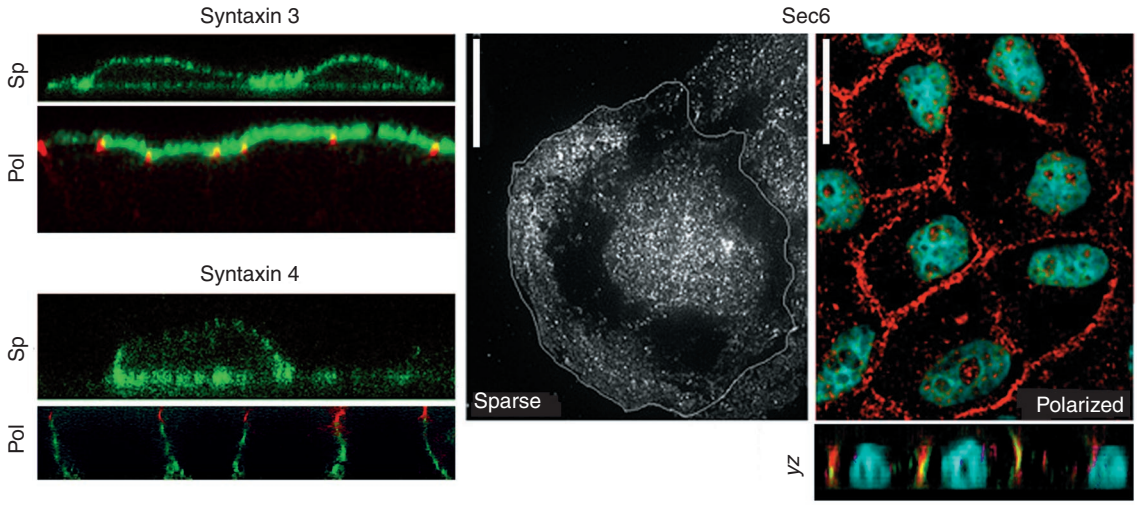

Figure 2 **Localization of Syntaxins 3 and 4 and Sec6 in MDCK cells.** The steady state, surface distribution of Syntaxins 3 and 4 (green) in sparse and polarized MDCK cells was determined by immunostaining for the extracellular Myc epitope fused to Syntaxins 3 and 4. The tight junction marker, ZO-1 (red) was costained as a reference for cell–cell boundaries. Images of polarized cells are *z* sections through either confocal (syntaxins) or wide-field (Sec6) images taken at sequential focal planes. The distribution of Sec6 at the basal membrane of non-polarized cells was visualized using TIR-FM. In polarized cells, Sec6 (red) was present in the lateral membrane (*xy* view, top) and often colocalized with E-cadherin (green, *yz* view, bottom). DAPI-stained nuclei are shown in blue. Scale bars represent 20 μm.

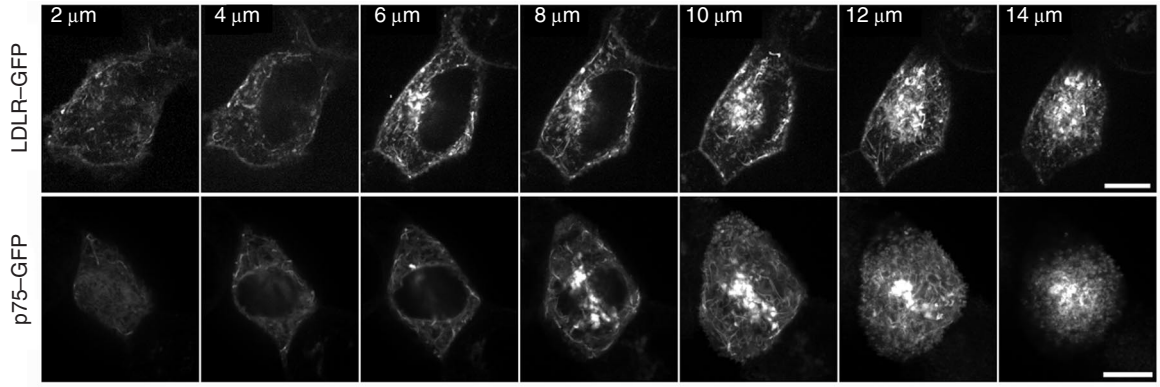

Figure 3 **Post-Golgi carrier movements are restricted within the apical cytoplasm.** The spatial distribution of post-Golgi carriers in polarized cells was determined using confocal time-lapse imaging in sequential *z*-axis planes. Time projections from 1-min recordings made at 2, 4, 6, 8, 10, 12 and 14 μm above the basal membrane are shown in cells expressing LDLR–GFP (34–50 min after release of the Golgi block) or p75–GFP (14–30 min after release of the Golgi block). Time-lapse images were recorded using identical acquisition settings and are displayed using identical display settings. The distribution of basolateral and apical PGTIs shown here was observed in 28 cells injected with LDLR–GFP and 23 cells injected with p75–GFP recorded during two independent experiments. Corresponding time-lapse recordings can be seen in Supplementary Information, Movie 2. Scale bars represent 10 μm.

plasma membrane in polarized epithelial cells.

Results

Apical or basolateral post-Golgi carriers fuse with the basal membrane in non-polarized MDCK cells. Proteins that are restricted to apical or basolateral membranes in polarized MDCK cells are often found on all cell surfaces in non-polarized cells. As at least some apical and basolateral proteins are sorted and packaged into different PGTIs in non-polarized epithelial cells[3], the non-restricted distribution of these markers could potentially be attributed to two processes: first, diffusion of apical and basolateral proteins throughout the cell surface after targeted delivery to presumptive apical and basolateral membranes (before the formation of tight junctions); second, to non-targeted surface delivery of apical and basolateral proteins. To examine these possibilities, we used TIR-FM to assess whether apical and basolateral PGTIs fuse with the plasma membrane domain that makes contact with the coverslip (hereafter referred to as the 'basal' plasma membrane). We expressed the green fluorescent protein (GFP)-tagged apical membrane protein p75 neurotrophin receptor (p75–GFP) and the GFP-tagged basolateral membrane proteins neural cell adhesion molecule (NCAM–GFP) or internalization-defective low-density lipoprotein receptor mutant (LDLR-A18–GFP) by injecting cDNAs into the nucleus of non-polarized or polarized MDCK cells[9]. During a 20 °C incubation, newly synthesized membrane proteins

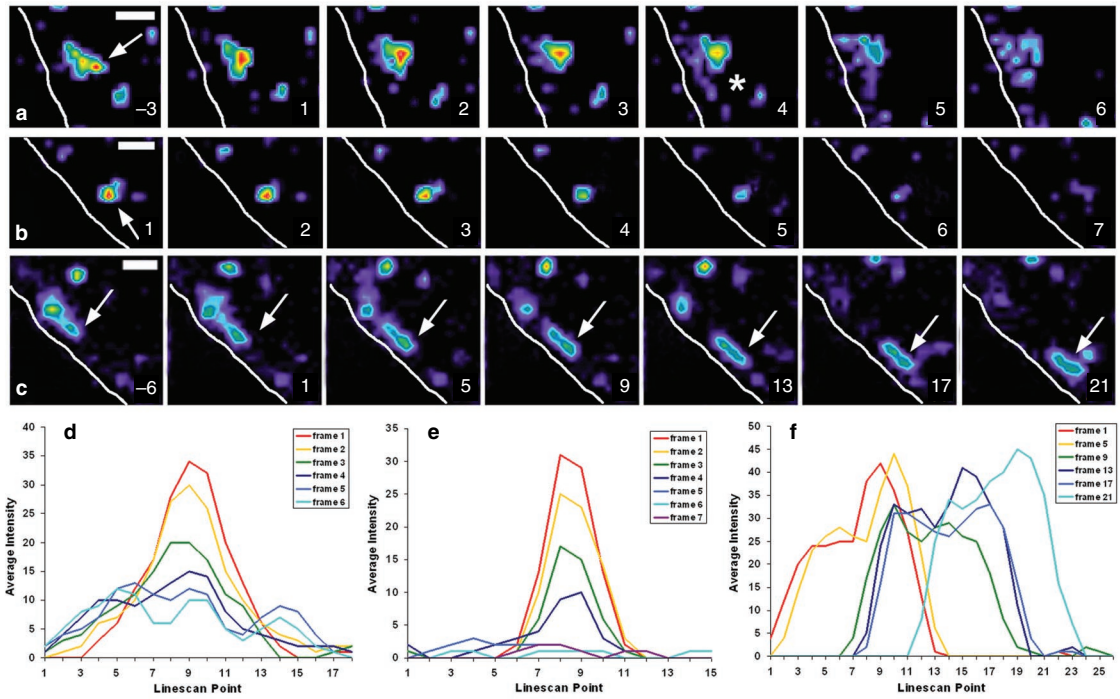

Figure 4 **Fusion of basolateral PGTIs with the lateral membrane in polarized MDCK cells.** PGTIs travelling through the cytoplasm to the plasma membrane exhibited different behaviours after making contact with the lateral membrane, each of which was represented by a different linescan intensity profile. Panels in **a–c** show selected images from time-lapse sequences (acquired between 15 and 53 min after release from the Golgi temperature block), illustrating these behaviours for PGTIs containing LDLR–GFP. White lines demarcate the extracellular boundaries of the plasma membrane with the cytoplasm always to the right of the lines. Arrows denote the PGTI of interest. Corresponding graphs in **d–f** show the measured linescan intensity profiles for each of the PGTIs in **a–c**, respectively. **a** and **d** show a fusing PGTI. The asterisk denotes the image frame at which a spread in carrier fluorescence was first visible. Note, however, that the linescan shows spreading began in the previous frame. **b** and **e** show a PGTI moving out of the plane of focus after contacting the membrane. **c** and **f** show a PGTI moving along the membrane without leaving the focal plane. Frame numbers refer to the time-lapse image plane at the start of each PGTI event. Image frames were enlarged and pseudocoloured for clarification. Scale bars represent 1 μm.

accumulated in a perinuclear compartment (Fig. 1a, wide field), defined as Golgi/TGN by colocalization with newly synthesized galactosyl transferase–cyan fluorescent protein (CFP; data not shown). After release from the temperature block, all three markers acquired a homogeneous distribution in non-polarized cells and distinctive apical or basolateral distributions in polarized cells (Fig. 1a).

Using TIR-FM, PGTIs containing GFP-tagged fusion proteins are detected only when they move into an evanescent field, which in our experiments was within ~120nm of the basal membrane. Previously, we established a quantitative method for detecting *bona fide* fusion of PGTIs with the plasma membrane[20]. In time-lapse TIR-FM recordings (500 frames, ~4 frames s^{-1}) made in non-polarized MDCK cells after release from a Golgi temperature block, we observed fusion of 57 PGTIs containing p75–GFP (Fig. 1a and Supplementary Information, Movie 1), 42 PGTIs containing LDLR-A18–GFP (Fig. 1a) or 27 PGTIs containing NCAM–GFP with the basal membrane (circles demarcate positions of fusion events). Accompanying movies can be found at http://www.boulan-lab.acomhosting.com. Fusing PGTIs displayed both vesicular and tubular morphologies (Fig. 1b) and could often be observed moving along the basal membrane in TIR-FM movies. Images shown in Fig. 1 and Supplementary Information Movies are representative of time-lapse recordings from at least three independent experiments monitoring exocytosis of each of the GFP-tagged cargoes. Fusion of post-Golgi carriers with the plasma membrane began within 5 min after release of the Golgi temperature block and continued for 60–70 min (NCAM–GFP) or for up to 2 h (LDLR-A18–GFP or p75–GFP). In all cases, the cessation of plasma membrane fusion correlated directly with the emptying of GFP markers from the Golgi, as detected by wide-field illumination. These results demonstrate that the uniform surface distribution of apical and basolateral markers is caused by non-targeted membrane delivery before MDCK polarization. The observed difference in rates of Golgi emptying for each of the markers, and the fact that co-expressed apical and basolateral proteins fused to cyan or yellow fluorescent protein were often segregated into different PGTIs (data not shown and ref. 3) further supports the idea that protein sorting in the Golgi occurs in non-polarized MDCK cells. Neither LDLR-A18 (ref. 36), p75 (ref. 37) nor NCAM[38] are efficiently recycled from the plasma membrane into the endosomal system (see Supplementary Information, Fig. S3). Thus, the fusion events we report probably represent direct delivery of Golgi-derived secretory carriers to the plasma membrane.

Fusion of post-Golgi carriers with the basal membrane is abrogated by cell polarization. In contrast to non-polarized cells (in which PGTIs fused with an averaged rate of 0.25–0.5 fusions s^{-1} $cell^{-1}$), in polarized cells, we did not detect fusion of a single apical or basolateral PGTI with the basal membrane (Fig. 1a, polarized, TIR-FM). Despite the lack of detectable fusion events using TIR-FM, wide-field illumination clearly showed that p75–GFP (Fig. 1a, polarized, wide field) accumulated in the apical membrane, while both LDLR-A18–GFP (Fig. 1a, polarized, wide field) and

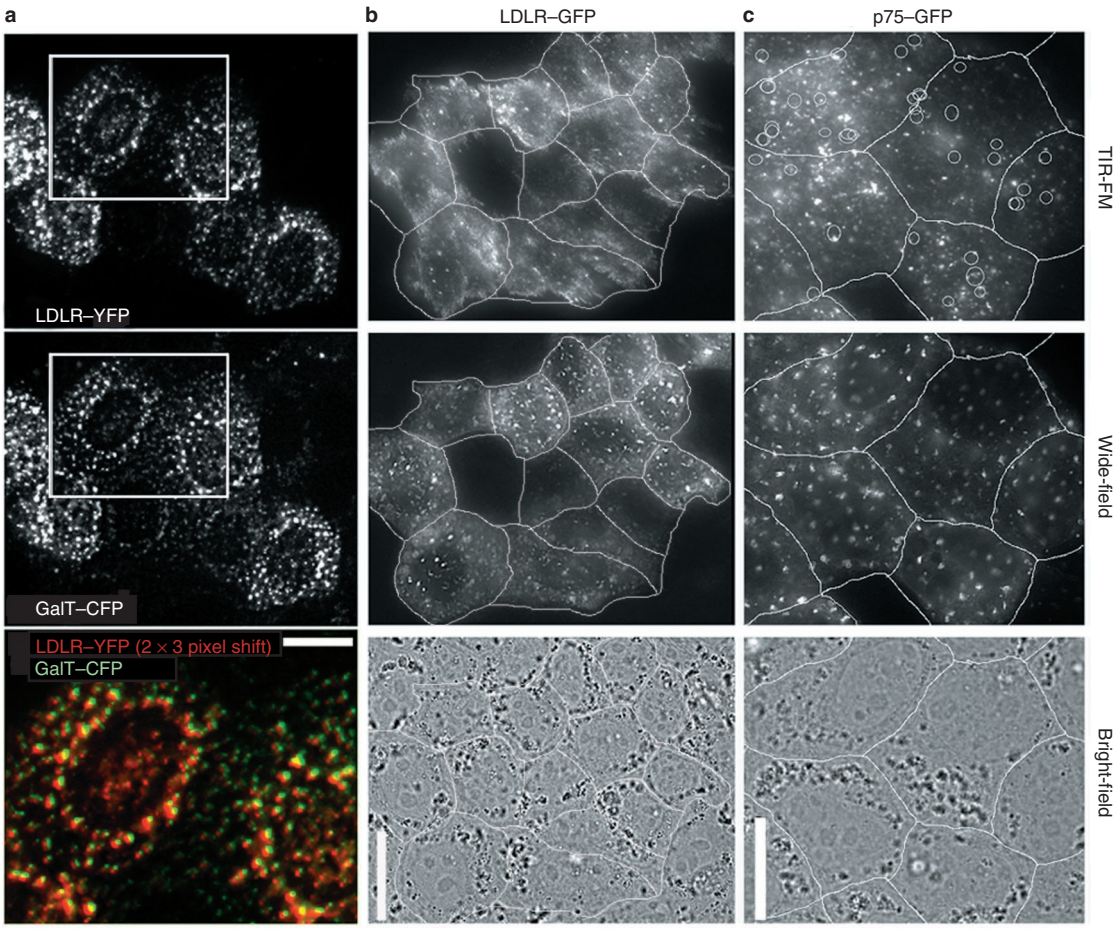

Figure 5 **Microtubule disruption selectively promotes fusion of apical PGTIs with the basal membrane.** TIR-FM was used to monitor fusion of transport intermediates with the plasma membrane in nocodazole-treated, polarized MDCK cells. Nocodazole induces fragmentation and scattering of the Golgi/TGN (as detected by the presence of GalT–CFP in **a**), but does not block accumulation of newly synthesized membrane proteins (LDLR-A18–YFP in **a** and p75–GFP in panel **b**, wide-field) in the Golgi during a 20 °C block. Colocalization of GalT–CFP and LDLR-A18–YFP after incubation at 20 °C is demonstrated in the colour overlay; the LDLR–YFP image was shifted down and left (2 × 3 pixels) to best illustrate the degree of colocalization. Circles in the TIR-FM image of p75–GFP show where PGTIs containing p75–GFP fused with the basal membrane (see Supplementary Information, Movie 4; 6 min after release of the Golgi block). Wide-field images in **b** and **c** are three-dimensional projections of serial *z*-axis images after release from the Golgi temperature block. No fusion events were detected by TIR-FM in nocodazole-treated cells expressing LDLR–GFP (**b**, 14 min after release of the Golgi block). Cell boundaries were demarcated using bright-field images as a reference (**b**, bright-field). Scale bar represents 15 μm.

NCAM–GFP (data not shown) accumulated in the lateral membrane during the course of our recordings. Interestingly, although we detected no fusion of basolateral PGTIs, TIR-FM identified some basolateral carriers moving in close proximity with the basal membrane. Thus, although some basolateral PGTIs can reach the basal membrane, in polarized cells, this membrane is not fusion competent. These results show that after epithelial cell polarization, fusion of post-Golgi carriers is restricted to regions of the plasma membrane other than the basal domain.

Sites of exocytosis correspond with the distribution of Syntaxin 3 and Syntaxin 4. Next, we examined whether changes in the distribution of the targeting and fusion machinery correlated with abrogation of basal fusion after MDCK polarization. We analysed the surface localization of the t-SNARES, Syntaxin 3 and 4, and the exocyst component, Sec6, in sub-confluent and fully polarized MDCK cells. In sparsely seeded cells, both Syntaxin 3 and 4 localized to all plasma membrane surfaces (Fig. 2, sparse). In polarized cells, however, neither syntaxin was present at the basal membrane. Instead, Syntaxin 3 localized exclusively to the apical membrane, whereas Syntaxin 4 was highly enriched in the lateral membrane (Fig. 2, polarized; also see ref. 33). In non-polarized cells, wide-field illumination revealed that Sec6 localizes to both the cytoplasm and punctate foci distributed throughout the cell periphery (data not shown). These Sec6 foci were present at, or near, the basal membrane, as they could be imaged using TIR-FM (Fig. 2, sparse). In polarized cells, Sec6 localized exclusively along the lateral membrane and partially colocalized with E-cadherin (Fig. 2, polarized and *yz* view of polarized cells). Thus, fusion of apical and basolateral PGTIs to the basal membranes of non-polarized cells correlated with the basal localization of Sec6 and Syntaxins 3 and 4; however, abrogation of fusion to basal membranes in polarized cells correlated with a redistribution of Syntaxins 3 and 4 and Sec6 to apical or lateral membrane domains.

Apical and basolateral PGTIs are concentrated in the apical half of polarized MDCK cells. As neither apical nor basolateral PGTIs fused with the basal membrane of polarized MDCK cells, we wondered where PGTIs fuse after polarization. First, we studied the distribution of PGTIs in polarized cells by making time-lapse

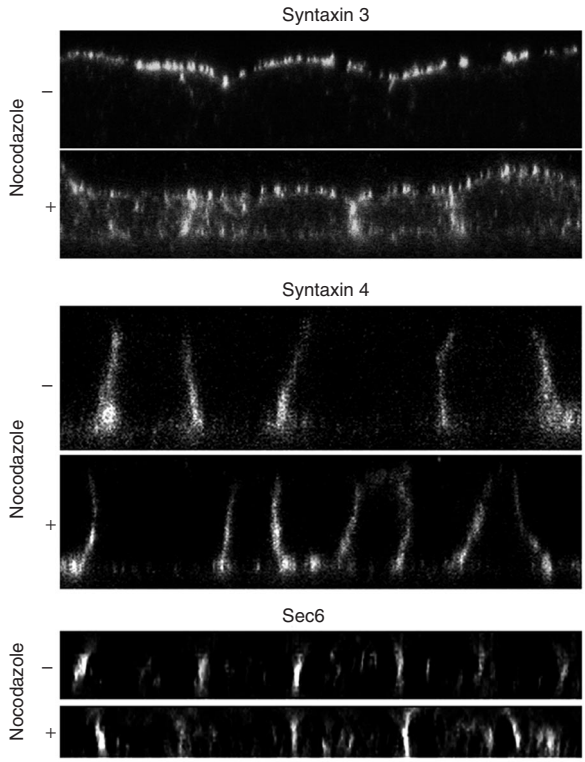

Figure 6 **Disruption of microtubules results in the selective depolarization of Syntaxin 3 in polarized MDCK cells.** Microtubules were depolymerized as described in Fig. 5. Cells stably transfected with Myc-tagged Syntaxins 3 or 4 were surface-labelled with an anti-Myc antibody. Note that Syntaxin 3 immunolocalizes to both apical and basolateral membranes after nocodazole-treatment, whereas the distribution of Syntaxin 4 is unaffected. Immunolabelling of endogenous Sec6 revealed that the distribution of this exocyst component is unaffected by microtubule perturbation.

Table 1 Three-dimensional distribution of lateral membrane fusion in polarized MDCK cells.

	LDLR–GFP				
	Cell 1	Cell 2	Cell 3	Cell 4	Total
μm from cell bottom					
14	0	0	0	0	0
12	4	3	2	2	11
10	2	1	5	3	11
8	3	2	3	1	9
6	4	5	3	0	12
4	0	0	0	0	0
2	0	0	0	0	0
0	0	0	0	0	0
Total	13	11	13	6	43

The number of PGTIs exhibiting an intensity profile indicative of fusion with the lateral membrane at various distances from the cell bottom were counted in four cells expressing the basolateral membrane protein LDLR-A-18–GFP. Intensity profiles representative of fusing PGTIs were only observed in time-lapse images acquired at 6, 8, 10 and 12 mm above the cell bottom.

confocal microscopy recordings at 2-μm *z*-axis intervals through polarized cells expressing p75–GFP, NCAM–GFP or LDLR-A18–GFP. Images were acquired at ~3.5 frames s^{-1} for a duration of 1 min at each *z* interval. In all experiments, MDCK cells were grown on glass coverslips and polarized cells reached an average height of 14 μm. The tall stature of polarized MDCK cells in our experiments directly reflects measuring cell height in living, rather than fixed, cells. Our recordings showed that trafficking PGTIs containing LDLR-A18–GFP (Fig. 3; also see Supplementary Information, Movie 2) or NCAM–GFP (data not shown) were concentrated in the cytoplasm, between 6–12 μm above the basal plasma membrane. In contrast, whereas Golgi membranes containing p75–GFP were observed between 8–12 μm above the basal membrane, PGTIs containing p75–GFP were most frequently observed between 10–12 μm above the basal membrane (Fig. 3, also see Supplementary Information, Movie 2). These apical PGTIs were mainly excluded from all other regions of the cytoplasm. Thus, PGTIs containing basolateral proteins had broader distributions than PGTIs containing apical proteins, which were restricted to a narrow band under the apical surface.

Basolateral, but not apical, PGTIs fuse with the lateral membrane. The different distribution of apical and basolateral PGTIs in polarized cells suggested that they might fuse with different domains of the plasma membrane. We utilized time-lapse confocal microscopy, as described above, to evaluate if, and where, apical or basolateral carriers fuse with the lateral membrane. We analysed changes in the total fluorescence intensity over time of small (5 × 5 pixels), consecutive regions drawn throughout the entire lateral membrane at each *z* interval imaged. Approximately 60 individual membrane regions were analysed per cell at each focal plane. When PGTIs entered a membrane region of interest (ROI), there was always an increase in the total fluorescence intensity at that ROI. In cells expressing LDLR-A18–GFP, an average of 17 ± 12 of the 60 membrane ROIs per focal plane (at focal planes 2–12 μm above the cell bottom) exhibited a transient increase in total fluorescence over time. Similarly, in cells expressing p75–GFP, an average of 15 ± 9 membrane ROIs per focal plane (at focal planes 8–12 μm above the cell bottom) exhibited a transient increase in total fluorescence over time. As apical PGTIs were almost entirely excluded from the bottom half of the cytoplasm (see above), we detected very few changes in fluorescence intensity at membrane ROIs in focal planes 2–6 μm from the cell bottom. A subsequent decrease in fluorescence intensity at the same membrane ROI could be attributed to one of four possible events: first, fusion of the PGTI with the membrane; second, movement of the PGTI out of the focal plane (Δ-*z*); third, movement of the PGTI away from the ROI in the plane of focus (Δ-*xy*); fourth, either a combination of fusion with movement out of the focal plane or movement in both *xy* and *z* axes.

To discriminate between these possibilities, each membrane ROI displaying a transient increase in fluorescence intensity clearly above the noise was screened by linescan analysis (see Methods). Analysis of PGTIs ($n = 235$) moving near the plasma membrane revealed linescan profiles characteristic of all four behaviours described above. Analysis of PGTIs moving in the cytoplasm near the cell centre ($n = 20$) revealed profiles characteristic of carriers either moving out of the focal plane, moving in the plane of focus without fusing or moving in both the *xy* and *z* axes (see Supplementary Information, Fig. S1c and S1c′), but none were characteristic of PGTIs fusing with the plasma membrane. Only linescan profiles exhibiting a decrease in total intensity, concomitant with an increase in the width of fluorescence intensity along the line being measured at the membrane, were counted as fusion events in our analysis. This profile probably represents fusion of a PGTI with the plasma membrane and subsequent diffusion of its

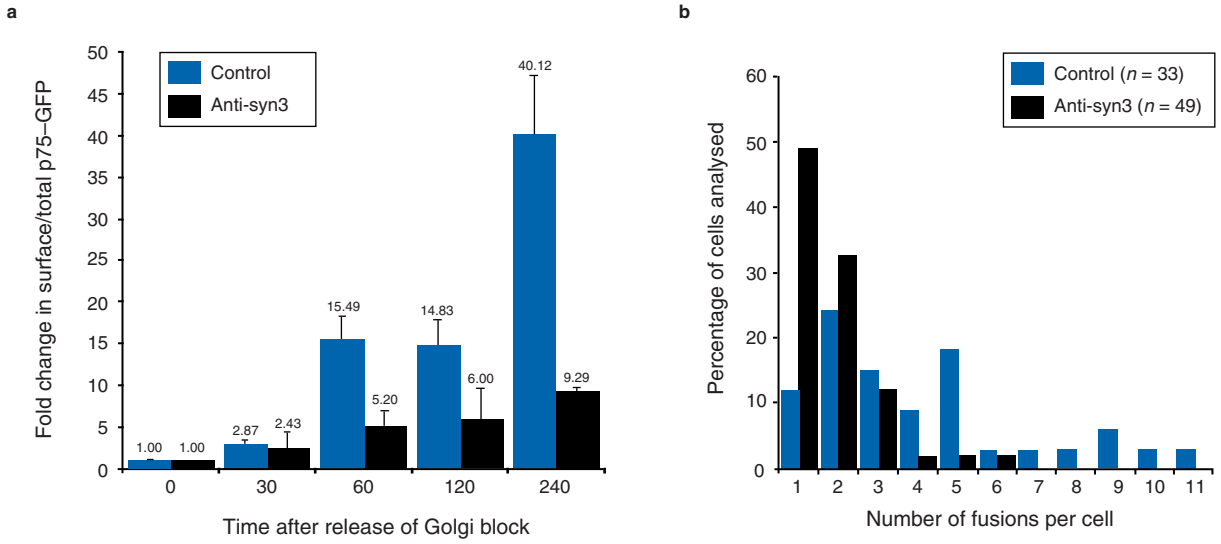

Figure 7 **Micro-injected Syntaxin 3 antibody inhibits fusion of apical PGTIs with the basal membrane in nocodazole-treated, polarized cells.** Untreated (**a**) or nocodazole-treated (**b**) cells were co-injected with p75–GFP cDNA and either a control antibody or an anti-Syntaxin 3 antibody. **a**, Delivery of p75–GFP to the apical membrane of control polarized cells was analysed by measuring the relative amount of surface-immunolabelled p75–GFP to total p75–GFP over time. The graph shows the fold change in surface:total GFP in cells micro-injected with control antibody or an anti-Syntaxin 3 antibody after release from the Golgi temperature block. Error bars represent the standard deviation of results from two independent experiments. **b**, Fusion of PGTIs containing p75–GFP with the basal membrane was monitored by TIR-FM between 15 and 50 min after release from the Golgi temperature block. Fusion events were counted in 33 (control antibody) and 49 (Syntaxin 3 antibody) cells imaged in 1500-frame time-lapse recordings. Images were acquired at 5 frames s^{-1}. The graph shows the percentage of cells in which 1–11 fusion events were detected at the basal membrane. Only cells in which we detected at least one fusion event were counted in this analysis. Data were compiled from three independent experiments.

fluorescent cargo (Fig. 4a, d; also see Supplementary Information, Movie 3 and Fig. S1a). An increase in the width of PGTI fluorescence intensity is one of the criteria for quantitatively defining fusion by TIR-FM[20]. These profiles were only observed for PGTIs that contacted the plasma membrane. This indicates that linescan profiles showing an increase in the width of fluorescence intensity exemplify events unique to PGTI–plasma membrane interactions, such as membrane fusion. Thus, only events exhibiting this profile were counted as fusion events in the quantitative analysis shown below.

Using this analysis on cells expressing LDLR-A18–GFP (four cells from two independent experiments), we identified 43 PGTIs whose fluorescence intensity profile indicated that the carrier had fused with the plasma membrane. All of these events occurred at approximately equal frequencies within four confocal planes imaged between 6–12 μm from the basal membrane (Table 1). We observed an additional 67 PGTIs with linescan profiles representative of either simultaneous fusion and movement of the carrier in the *xy* and/or *z* axes or movement of the carrier in both *xy*- and *z*-axes without fusion (see Supplementary Information, Fig. S1b, S1b′). These types of events were observed from 2–12 μm above the basal membrane. In an independent assay, fusion with the lateral membrane could also be identified when the colour of GFP-labelled PGTIs (green) transiently turned yellow as they fused with a $DiIC^{16}$-labelled (red) plasma membrane (see Supplementary Information, Fig. S2 and Movie 5). In contrast, in cells expressing p75–GFP (three cells from two independent experiments), we did not identify any PGTIs that could be considered to be fusing with the lateral membrane. The complete absence of membrane fusion for apical PGTIs could not be attributed to a reduced number of PGTIs coming into contact with the membrane, as cells expressing either p75–GFP or LDLR-A18–GFP contained a similar number of membrane regions exhibiting a transient change in total fluorescence intensity (see above). In addition, comparable numbers of PGTIs containing p75–GFP were observed moving through the apical cytoplasm (see Supplementary Information, Movie 2). Nor could it be attributed to a change in PGTI properties that rendered them undetectable, as measurements of apical carrier size, shape and cargo capacity were not significantly different in non-polarized and polarized cells (G.K. and E.R.B., unpublished observations).

In summary, the results of the experiments described above suggest that PGTIs carrying basolateral membrane proteins fuse selectively with the lateral plasma membrane. PGTIs containing an apical marker were not observed to fuse with the lateral membrane, suggesting that they fuse directly with the apical membrane.

Targeted fusion of apical, but not basolateral, PGTIs in polarized MDCK cells requires microtubules. The mechanism by which disruption of microtubules preferentially perturbs the asymmetric distribution of apical membrane proteins is not known. To investigate whether microtubules are involved in determining plasma membrane fusion sites of apical or basolateral PGTIs, we examined whether PGTIs fused with the basal membrane of polarized cells when microtubules were completely depolymerized. To depolymerize all microtubules, we incubated cells on ice in the presence of 20 μM nocodazole for 60 min before micro-injection. Cells were continuously incubated in 10 μM nocodazole for the duration of experiments to prevent re-assembly of microtubules. As previously described[39,40], nocodazole treatment resulted in fragmentation of the Golgi apparatus into numerous GalT–CFP-positive Golgi mini-stacks that were dispersed throughout the cell (Fig. 5a). This treatment affected neither expression nor Golgi accumulation of the GFP-tagged reporter proteins (Fig. 5a; colocalization of LDLR-A18–YFP with GalT–CFP). After incubation at 20 °C, Golgi mini-stacks containing either apical or basolateral GFP-tagged membrane proteins were visible in close proximity to the basal membrane by TIR-FM (Figs 5b, c). This is in

marked contrast to polarized cells with an intact microtubule array, in which the Golgi localizes to a supra-nuclear position and cannot be detected by TIR-FM (compare with Fig. 1). Additionally, in nocodazole-treated cells that were co-injected with p75–CFP and LDLR-A18–YFP, we found that apical and basolateral markers colocalized in Golgi mini-stacks during the 20 °C block, but emptied from the Golgi at different rates after release of block (data not shown). This indicates that the protein sorting activity of the Golgi/TGN is maintained in the absence of microtubules.

After release of the Golgi temperature block in nocodazole-treated cells, neither LDLR–GFP (Fig. 5b) nor NCAM–GFP (data not shown) could be detected fusing with the basal plasma membrane. In marked contrast, carriers containing p75–GFP fused with the basal membrane under these conditions (Fig. 5c; also see Supplementary Information, Movie 4, $n = 40$ fusions per 1000 frames). As both apical and basolateral carriers were detected by TIR-FM after nocodazole treatment, but only carriers containing p75–GFP fused with the basal membrane, our results show that exocytosis at the basal membrane is not caused by the proximity of redistributed Golgi elements with the basal cell surface. Rather, they show that sorting of apical and basolateral membrane proteins still occurs within scattered Golgi elements and that the basal membrane becomes fusion competent specifically for apical, but not basolateral, PGTIs after disruption of microtubules. The role of microtubules in targeted exocytosis of apical cargo could either be direct, by targeting delivery of apical PGTIs to the correct membrane domain, or indirect, by regulating the distribution of components of the targeting and fusion machinery for apical exocytosis.

Microtubule disruption results in a non-polarized distribution of Syntaxin 3. To elucidate the mechanism by which nocodazole selectively induces fusion of PGTIs containing p75–GFP with the basal membrane in polarized cells, we tested whether the localization of components of apical and basolateral tethering and fusion machineries were altered by disruption of microtubules. Nocodazole treatment resulted in a redistribution of Syntaxin 3 from the apical surface to both apical and basolateral membranes, but did not alter the distribution of Syntaxin 4 or Sec6 (compare Fig. 2 and Fig. 6, polarized cells). Nocodazole treatment does not disrupt the barrier function of tight junctions in MDCK cells[19], nor did it perturb the apicolateral distribution of zonula occludens 1 (ZO-1), a marker for the tight junction (data not shown). These results suggest that redistribution of Syntaxin 3 may be critical in facilitating exocytosis of apical cargo at the basal membrane after microtubule disruption.

To test whether Syntaxin 3 is permissive for fusion of apical PGTIs with the plasma membrane, we co-injected untreated or nocodazole-treated polarized cells with p75–GFP cDNA and either an antibody raised against the cytoplasmic domain of Syntaxin 3 or a control antibody. Delivery of p75–GFP to the apical membrane of cells with an intact microtubule array was assayed by measuring the ratio of cell-surface immunolabelled p75 (see Methods) to total p75–GFP in polarized cells at varying times after release of the Golgi block. In two independent experiments, micro-injection of Syntaxin 3 antibodies resulted in a 77 ± 3% reduction in the ratio of surface:total p75–GFP at the apical membrane 4 h after release from the Golgi, compared with cells micro-injected with control antibody (Fig. 7a). These data indicate that in MDCK cells, our anti-Syntaxin 3 antibody has function-blocking properties with respect to Syntaxin 3-mediated delivery of apical cargo to the plasma membrane. In nocodazole-treated cells, we evaluated the effect of Syntaxin 3 inhibition by comparing the number of fusion events observed by TIR-FM in single cells injected with control or Syntaxin 3 antibodies. In data combined from three independent experiments, we detected four or more fusion events in only 6% of the cells injected with anti-Syntaxin 3 antibodies, as compared with 49% of cells injected with control antibodies (Fig. 7b). These results show that Syntaxin 3 contributes directly to creating a plasma membrane environment permissive for fusion of apical PGTIs *in vivo*. Furthermore, they suggest that microtubules facilitate apical delivery of plasma membrane proteins by promoting a restricted apical distribution of Syntaxin 3.

Discussion

Advances in time-lapse fluorescence microscopy and the use of GFP-tagged chimaeras have facilitated the study of intracellular membrane trafficking along the biosynthetic pathway in non-polarized cells[3,8,9,20,41,42]. In this study, we used live-cell imaging techniques to study the trafficking and fusion of PGTIs with the cell surface in polarized MDCK cells. Our results provide fresh insights into how epithelial cells organize their exocytic machinery during the establishment of polarity.

Using TIR-FM, we show that PGTIs carrying apical or basolateral cargo can fuse with the basal membrane of non-polarized MDCK cells. These data are in agreement with results obtained in non-polarized PtK_2 epithelial cells[3]. Our results provide direct evidence that the uniform plasma membrane distribution of at least some apical and basolateral membrane proteins in non-polarized MDCK cells is caused by non-targeted delivery of PGTIs, rather than by targeted delivery and subsequent membrane diffusion in the absence of tight junctions. Additionally, we made the observation that exocytosis of both apical and basolateral membrane proteins at the basal plasma membrane is completely abrogated after MDCK cells polarize. As wide-field illumination revealed that apical and basolateral proteins accumulated in the correct plasma membrane domain, the loss of basal fusion indicated activation of a polarization-dependent mechanism for redirecting PGTIs to different regions of the cell surface. Indeed, sequential *z*-axis recordings of post-Golgi trafficking revealed a spatial segregation of apical and basolateral carriers emerging from the Golgi complex; apical PGTIs were localized primarily in the uppermost 4 μm of the cytoplasm, whereas basolateral PGTIs were broadly distributed throughout central regions of the cytoplasm. The restricted distribution of apical PGTIs may be attributed to an association with the sub-apical microtubule array. In contrast, the wider distribution of basolateral PGTIs could reflect their emergence from an apically localized Golgi complex and association with more broadly distributed cytoskeletal elements.

Using time-lapse confocal microscopy, we were able to quantitatively analyse whether basolaterally targeted PGTIs containing either LDLR–GFP or NCAM–GFP fused with the lateral membrane. Fluorescence intensity profiles characteristic of fusing PGTIs were only observed in central and apical domains of the lateral membrane. This is consistent with the observation that basolateral PGTIs were concentrated in central and apical regions of the cytoplasm. Although a variety of biochemical assays have demonstrated a direct pathway from the Golgi to the basolateral membrane[43–45], they inherently cannot discriminate whether exocytosis occurs throughout the basolateral membrane or at specific regions of this membrane. In contrast, our microscopy-based assays clearly demonstrate that basolateral carriers are targeted exclusively to the lateral domain of the basolateral membrane for exocytosis. To our knowledge, these experiments are the first direct demonstration of targeted exocytosis in polarized epithelial cells.

We did not observe fluorescence intensity profiles characteristic of fusing carriers at either the basal or lateral membrane in polarized cells expressing the apical marker, p75–GFP. The lack of detectable fusion events for apical PGTIs, despite their abundance in the cytoplasm and the accumulation of p75–GFP at the apical surface, suggests that they fuse directly with the apical membrane. This interpretation is consistent with domain-selective, surface labelling data showing that newly synthesized ^{35}S-methionine-labelled p75–GFP is delivered directly to the apical membrane in polarized MDCK cells[9]. Although PGTIs containing p75–GFP do not fuse with the lateral membrane, PGTIs carrying other apical

proteins may be capable of lateral membrane fusion in polarized cells. In the future, it will be interesting to address this using cells expressing proteins delivered to the apical membrane via the indirect, transcytotic route, as well as in cells expressing apical proteins dependent on inclusion into lipid rafts for their delivery to the apical surface.

Abrogation of exocytic events at the basal plasma membrane and redirection to the lateral membrane after polarization correlated with changes in the distribution of molecular components of the apical and basolateral fusion machineries. Basal fusion of PGTIs occurred in non-polarized cells when Syntaxins 3 and 4 were present at the basal membrane but was never observed in polarized cells where both syntaxins were absent from the basal membrane. These results suggest that Syntaxins 3 and 4 must be present in target membranes for fusion of apical and basolateral PGTIs to occur. Syntaxin 3-dependent delivery of apical proteins was confirmed by the measured inhibition in delivery of p75–GFP to the apical or basal membrane in untreated or nocodazole-treated cells, respectively, when cells were injected with an antibody against the cytoplasmic domain of Syntaxin 3. Syntaxin 4-dependent fusion of basolateral PGTIs was suggested by the restricted lateral localization of both Syntaxin 4 and fusion of basolateral PGTIs. These data are consistent with the concept that t-SNAREs are necessary for fusion of PGTIs, but do not rule out the possibility that additional factors, such as tethering proteins, are also involved in domain-specific targeting of some PGTIs[46–49]. One of these additional factors is the exocyst, which localizes along the lateral membrane in our cells and was recently demonstrated to have an important role in basolateral membrane trafficking in MDCK cells[31,32]. The imperfect codistribution of basolateral PGTIs fusing at the lateral membrane with Syntaxin 4 and Sec6 might be attributed to the fact that fusion events were monitored in living cells, whereas Syntaxin 4 and Sec6 were localized in fixed cells by immunocytochemistry.

Finally, we found that in polarized cells, apical PGTIs regained the ability to fuse with the basal membrane after depolymerization of microtubules. This mis-targeting of p75–GFP to the basal membrane correlated with mis-localization of Syntaxin 3 at the basal membrane in response to treatment with microtubule antagonists. It has previously been shown that antibodies against Syntaxin 3 inhibit delivery of influenza haemagglutinin (HA) to the apical surface in permeabilized MDCK cells[35]. Similarly, we found that micro-injected Syntaxin 3 antibodies inhibited delivery of p75–GFP to the apical surface in intact cells (Fig. 7a). Strikingly, nocodazole-induced fusion of apical PGTIs with the basal membrane was also partially inhibited by injected Syntaxin 3 antibodies, suggesting that mis-localization of Syntaxin 3 causes the basal membrane to become fusion-competent for apical PGTIs after disruption of microtubules. The incomplete inhibition of basal fusion by Syntaxin 3 antibodies could reflect either incomplete inhibition by the antibody or the participation of another factor(s) in mediating fusion of apical PGTIs with the membrane under these conditions. In contrast, microtubule depolymerization did not promote fusion of PGTIs containing either LDLR–GFP or NCAM–GFP with the basal membrane, nor did it result in redistribution of Syntaxin 4 or exocyst components to the basal membrane. The mechanism by which t-SNAREs are targeted to different membrane domains in polarized cells is unclear. Our finding that the localization of Syntaxin 3, but not Syntaxin 4, is sensitive to microtubule depolymerization demonstrates that t-SNARE distributions are differentially controlled by microtubules *in vivo*. These results provide mechanistic insight into previous findings showing that microtubules are preferentially involved in controlling the apical targeting of membrane proteins in epithelial cells[18,19,21–28]. □

Methods

Cell culture and micro-injection

MDCK cells were maintained in DMEM (Invitrogen, Carlsbad, CA) supplemented with 10% foetal bovine serum (FBS) in a 37 °C incubator humidified with 5% CO_2. For analysis of non-polarized cells, MDCK cultures were seeded at a density of ~13,000 cells cm^{-2} onto heat-sterilized 25 mm round coverslips and grown for 36 h before micro-injection. For polarized cell analyses, cells were seeded at a density of ~130,000 cells cm^{-2} and grown for 4–5 days to ensure the formation of a fully polarized monolayer before micro-injection. Cells were pressure micro-injected intranuclearly with cDNAs prepared in HKCl micro-injection buffer (10 mM Hepes, 140 mM potassium chloride at pH 7.4); 5 μg ml^{-1} for p75–GFP, 20 μg ml^{-1} for NCAM–GFP and 15 μg ml^{-1} for LDLR-A18–GFP, using back-loaded glass capillaries and a Narishige micromanipulator (Narishige, Greenvale, NY). Rabbit polyclonal antibodies raised against a GST fusion protein of the full-length carboxy-terminal cytoplasmic tail of rat Syntaxin3 have been described previously[50]. The anti-Syntaxin 3 antibody was purified from rabbit serum, as previously described[9]. Control and Syntaxin 3 antibodies were concentrated by vacuum dialysis in HKCl injection buffer and micro-injected at a final concentration of 11 mg ml^{-1}. Injected antibody could be detected in cells after fixation and staining with fluorescently conjugated anti-rabbit antibody (Jackson ImmunoResearch, West Grove, PA). After injection, cells were maintained at 37 °C in a humidified CO_2 environment for 60 min to allow for expression of injected cDNAs. Newly synthesized protein was accumulated in the TGN by incubating cells at 20 °C in bicarbonate-free DMEM supplemented with 5% FBS, 20 mM Hepes and 100 μg ml^{-1} cycloheximide (Sigma, St Louis, MO). Before release of the 20 °C block no significant amount of LDLR-A18–GFP, NCAM–GFP or p75–GFP could be detected at the cell surface, as determined by surface immunolabelling of unpermeabilized paraformaldehyde-fixed cells. Cells were transferred to recording medium (Hanks Balanced Salt Solution, without phenol-red, supplemented with 20 mM HEPES, 1% FBS, 4.5 g l^{-1} glucose, essential and non-essential amino acids and 100 μg ml^{-1} cycloheximide) and the transport and fusion of post-Golgi carriers was monitored by time-lapse fluorescence microscopy after shifting to the permissive temperature for transport out of the Golgi (32 °C).

Microtubule depolymerization

Before micro-injection, cells were incubated in bicarbonate-free DMEM supplemented with 5% FBS and 20 mM Hepes on ice for 30 min to depolymerize the cold-labile, nocodazole-resistant microtubule population. Nocodazole (Sigma) was added to a final concentration of 20 μM and the cells were incubated for another 30 min on ice. This treatment completely depolymerized all microtubules (data not shown). cDNAs were then micro-injected and cells were treated as described above, except that they were maintained in 10 μM nocodazole for the remainder of each experiment to prevent re-assembly of the microtubule cytoskeleton.

DiIC^{16} plasma membrane labelling

Cells were micro-injected as described. Fluorescently labelled DiIC^{16} (Molecular Probes, Eugene OR) was added (50 μM final concentration) to bicarbonate-free DMEM without serum, supplemented with 20 mM Hepes and 100 μg ml^{-1} cycloheximide. DiIC^{16}-containing medium was added to the cells during the final 30 min of the Golgi temperature block. Cells were then washed three times with recording medium before dual-wavelength, confocal time-lapse imaging.

Plasmid construction

The cDNA encoding full-length NCAM in pBKCMV was a gift from J. Bruses (Memorial Sloan Kettering Cancer Center, New York, NY). PCR was used to introduce a *Kpn*I site at the NCAM 5′ end. The resulting PCR product was subcloned into pBKCMV-NCAM to create full-length NCAM without a stop codon. This construct was subcloned into the *Sal*I and *Kpn*I sites of pEGFP-N1 (Clontech, Palo Alto, CA) to generate NCAM-pEGFP-N1. The cDNA encoding LDLR-A18 (ref. 36) in pCB6 was provided by Karl Matter (University College of London, London, UK). PCR was used to introduce an *xma*I site at the 5¢ end. The resulting PCR product was subcloned into pBluescript-LDLR-A18, creating a full length LDLR-A18 without a stop codon. This construct was subcloned into the *Kpn*I and *xma*I sites of pEGFP-N1, to generate LDLR-A18–GFP. The construction of p75–GFP cDNA has been described previously[9]. cDNAs for human Syntaxins 3 and 4 were cloned into a modified pcDNA4/TO vector (Invitrogen) to add two C-terminal Myc epitope tags in tandem and one hexa-histidine tag to the C termini. MDCK cells were stably transfected and individual clones were used for this study. The additional epitope tags did not interfere with the correct polarized targeting of the Syntaxins and allowed detection at the plasma membrane by surface immunolabelling.

Indirect immunofluorescence

For Syntaxin 3 and 4 surface staining, MDCK cells transfected with tetracycline-inducible, Myc-tagged Syntaxin 3 or 4 were washed three times in ice-cold phosphate-buffered saline containing calcium (1 mM) and magnesium (1 mM) (PBS-CM), placed on ice and incubated with an anti-Myc monoclonal antibody (9E10 ascites, Santa Cruz Biotechnology, Santa Cruz, CA) for 2 h. Cells were washed in PBS-CM and fixed in freshly prepared 3% paraformaldehyde for 20 min on ice. Cells were permeabilized in PBS-CM with 0.1% Triton X-100 for 10 min at room temperature. The tight junction marker, ZO-1, was immunolabelled by incubating cells for 30 min at room temperature with a rat monoclonal antibody (Chemicon, Temecula, CA). Cells were subsequently labelled with appropriate fluorescently conjugated secondary antibodies (Jackson ImmunoResearch). For Sec6 immunostaining, cells were fixed in −20 °C methanol for 3 min or in 3% paraformaldehyde on ice for 15 min before permeabilization in 0.1 M Tris-HCl at pH 7.5 containing 0.05% SDS for 10 min at room temperature. Samples were then stained with a mouse monoclonal antibody against rSec6 (StressGen, Victoria, BC).

Quantification of p75–GFP at the cell surface

Groups of polarized cells were injected with p75–GFP cDNA and anti-Syntaxin 3 or control antibody. Cells were incubated for 1 h at 37 °C to allow expression of p75–GFP and then p75–GFP was accumulated in the Golgi by incubation at 20 °C for 2.5 h. Cells were shifted to 37 °C and fixed 0, 30, 60, 120 and 240 min after release of the Golgi temperature block in 2% paraformaldehyde at room temperature for 2 min. p75–GFP at the cell surface was immunolabelled with a monoclonal antibody that recognizes an extracellular epitope of p75, as described previously[9]. Cells were subsequently labelled with Cy3-conjugated anti-mouse antibodies. Images were acquired using a Nikon TE-300 microscope and a back-illuminated, cooled, charge-coupled-device camera (CCD 512X512-EBFT, Princeton

Instruments). Images of p75–GFP and anti-p75-injected cells were acquired using identical acquisition settings and exposure times for all samples in a single experiment. The integrated fluorescence intensities in GFP and anti-p75 images was measured and the ratio of anti-p75:p75–GFP intensities was calculated for each group of injected cells. The integrated fluorescence of 40–60 injected cells was measured at each time point.

Total internal reflection fluorescence microscopy (TIR-FM).

The prism-less TIR-FM was set up on an Olympus microscope (IX-70, Olympus America Inc.) as previously described[20] using a high numerical aperture lens (Apochromat 60×, NA 1.45, Olympus), resulting in an evanescent field with a decay length between 70 and 120 nm. In all TIR-FM recordings, we acquired 500-frame time-lapse sequences at ~4 frames s^{-1} (222-ms exposures), except as noted in Table 2. Images were acquired without binning, using a 12-bit cooled CCD (ORCA I, C4742-95, Hamamatsu) with 6.7-μm pixels. The camera was controlled by in-house software written in Labview 5.1 using the IMAQ Vision package (National Instruments, Austin, TX). Analysis of carrier fusion was performed as described[20]. Briefly, carrier fusion is defined by a simultaneous increase in both the total PGTI fluorescence intensity and the area occupied by carrier fluorescence as the carrier flattens into the plasma membrane and the cargo diffuses laterally. These criteria make it possible to distinguish fusing carriers from those moving near the plasma membrane or those that lyse.

Time-lapse confocal microscopy

After micro-injection and a 20 °C Golgi block, cells were transferred to a thermal-controlled recording chamber mounted on a Zeiss Axiovert 100 microscope (Carl Zeiss, Oberkochen, Germany) equipped with an UltraView spinning disc confocal head (Perkin Elmer, Shelton, CT). Spinning disc confocal recordings were made at the Rockefeller University Bioimaging Resource Center. The confocal depth was 1 μm and GFP was illuminated using the 488-nm argon laser. Images were collected using a 63× objective and the ORCA-ER, cooled CCD with 6.7-μm pixels (Hamamatsu, Bridgewater, NJ) with 2 × 2 binning. All imaging hardware was controlled by a workstation running MetaMorph imaging software (Universal Imaging, West Chester, PA). Time-lapse sequences were acquired at ~3.5 frames s^{-1} (200-ms exposures). Sequential time-lapse recordings were made at 2-μm *z*-intervals, starting at the bottom of the cell. Recording duration at each *z*-interval was 1 min. Post-acquisition analysis and processing of confocal images was performed using MetaMorph.

Lateral membrane fusion analysis

Adjacent 5 × 5 pixel regions were drawn along the entire lateral membrane of injected cells at each focal plane. The total fluorescence intensities in each region were measured for all frames. Regions of interest displaying transient increases in intensity above the noise level were subsequently screened for fusion by measuring the average fluorescence intensity at individual points on short lines drawn along the plasma membrane (linescan analysis). Before linescan analysis, all the frames from the time-lapse were averaged and the resulting averaged image was subtracted from each frame of the time-lapse. Subtraction of the averaged image resulted in elimination of the fluorescence signal contributed by non-moving structures (that is, the plasma membrane) enabling us to analyse selectively the fluorescence contributed by moving PGTIs. Linescan widths varied slightly from region to region and are displayed in the *x*-axis of graphs shown in Fig. 4. All image analysis was performed using MetaMorph. Several types of linescan profiles were observed: first, a decrease in total intensity concomitant with an increase in the width of fluorescence intensity along the line being measured at the membrane is representative of PGTI fusion with the plasma membrane and subsequent diffusion of its fluorescent cargo (Fig. 4a, d); second, a decrease in total intensity without an increase in the width of fluorescence intensity along the membrane. This profile was considered to be representative of carriers moving out of the plane of focus (Fig. 4b, e); third, a translocation of fluorescence along adjacent membrane regions without a significant change in either the total intensity or the width of fluorescence intensity. This profile clearly exemplifies PGTIs moving in the focal plane along the membrane (Fig. 4c, f); fourth, a combination of the profiles described above. For example, some PGTIs moved along adjacent membrane regions concomitant with a decrease in their total fluorescence intensity (see Supplementary Information, Figs S1b, S1b′). The linescan profile generated from such PGTIs could represent either simultaneous fusion and movement of the carrier in the *xy* and/or *z* axes or movement of the carrier in both *xy*- and *z*-axes without fusion. As we could not unambiguously differentiate between these two possible activities, they were not counted as fusion events. Only those carriers whose total fluorescence intensity decreased concomitant with an increase in the width of fluorescence intensity over time were considered to be fusing with the lateral membrane.

RECEIVED 1 APRIL 2002; REVISED 21 AUGUST 2002; ACCEPTED 5 DECEMBER 2002; PUBLISHED 27 JANUARY 2003.

1. Rodriguez-Boulan, E. & Nelson, W. J. Morphogenesis of the polarized epithelial cell phenotype. *Science* **245,** 718–725 (1989).
2. Simons, K. & Wandinger-Ness, A. Polarized sorting in epithelia. *Cell* **62,** 207–210 (1990).
3. Keller, P., Toomre, D., Diaz, E., White, J. & Simons, K. Multicolour imaging of post-Golgi sorting and trafficking in live cells. *Nature Cell Biol.* **3,** 140–149 (2001).
4. Rodriguez-Boulan, E. & Gonzalez, A. Glycans in post-Golgi apical targeting: sorting signals or structural props? *Trends Cell Biol.* **9,** 291–294 (1999).
5. Chuang, J. Z. & Sung, C. H. The cytoplasmic tail of rhodopsin acts as a novel apical sorting signal in polarized MDCK cells. *J. Cell Biol.* **142,** 1245–1256 (1998).
6. Le Gall, A., Yeaman, C., Muesch, A. & Rodriguez-Boulan, E. Epithelial cell polarity: new perspectives. *Sem. Nephrol.* **15,** 272–284 (1995).
7. Ikonen, E. & Simons, K. Protein and lipid sorting from the *trans*-Golgi network to the plasma membrane in polarized cells. *Semin Cell Dev Biol* **9,** 503–509 (1998).
8. Toomre, D., Keller, P., White, J., Olivo, J. C. & Simons, K. Dual-color visualization of *trans*-Golgi network to plasma membrane traffic along microtubules in living cells. *J. Cell Sci.* **112,** 21–33 (1999).
9. Kreitzer, G., Marmorstein, A., Okamoto, P., Vallee, R. & Rodriguez-Boulan, E. Kinesin and dynamin are required for post-Golgi *trans*port of a plasma-membrane protein. *Nature Cell Biol.* **2,** 125–127 (2000).
10. Bonifacino, J. S. & Dell'Angelica, E. C. Molecular bases for the recognition of tyrosine-based sorting signals. *J. Cell Biol.* **145,** 923–926 (1999).
11. Ohno, H. *et al.* The medium subunits of adaptor complexes recognize distinct but overlapping sets of tyrosine-based sorting signals. *J. Biol. Chem.* **273,** 25915–25921 (1998).
12. Kirchhausen, T. Adaptors for clathrin-mediated traffic. *Annu. Rev. Cell Dev. Biol.* **15,** 705–732 (1999).
13. Kirchhausen, T., Bonifacino, J. S. & Riezman, H. Linking cargo to vesicle formation: receptor tail interactions with coat proteins. *Curr. Opin. Cell Biol.* **9,** 488–495 (1997).
14. Noda, Y. *et al.* KIFC3, a microtubule minus end-directed motor for the apical *trans*port of annexin XIIIb-associated Triton-insoluble membranes. *J. Cell Biol.* **155,** 77–88 (2001).
15. Nakagawa, T. *et al.* A novel motor, KIF13A, *trans*ports mannose-6-phosphate receptor to plasma membrane through direct interaction with AP-1 complex. *Cell* **103,** 569–581 (2000).
16. Setou, M., Nakagawa, T., Seog, D. H. & Hirokawa, N. Kinesin superfamily motor protein KIF17 and mLin-10 in NMDA receptor-containing vesicle *trans*port. *Science* **288,** 1796–1802 (2000).
17. Bacallao, R. *et al.* The subcellular organization of Madin-Darby Canine Kidney cells during the formation of a polarized epithelium. *J. Cell Biol.* **109,** 2817–2832 (1989).
18. Gilbert, T., Le Bivic, A., Quaroni, A. & Rodriguez-Boulan, E. Microtubular organization and its involvement in the biogenetic pathways of plasma membrane proteins in Caco-2 intestinal epithelial cells. *J.Cell Biol.* **113,** 275–288 (1991).
19. Grindstaff, K. K., Bacallao, R. L. & Nelson, W. J. Apiconuclear organization of microtubules does not specify protein delivery from the *trans*-Golgi network to different membrane domains in polarized epithelial cells. *Mol. Biol. Cell* **9,** 685–699 (1998).
20. Schmoranzer, J., Goulian, M., Axelrod, D. & Simon, S. M. Imaging constitutive exocytosis with total internal reflection fluorescence microscopy. *J. Cell Biol.* **149,** 23–32 (2000).
21. Achler, C., Filmer, D., Merte, C. & Drenckhahn, D. Role of microtubules in polarized delivery of apical membrane proteins to the brush border of the intestinal epithelium. *J.Cell Biol.* **109,** 179–189 (1989).
22. Breitfeld, P. P., Mckinnon, W. C. & Mostov, K. E. Effect of nocodazole on vesicular traffic to the apical and basolateral surfaces of polarized Madin-Darby canine kidney cells. *J. Cell. Biol.* **111,** 2365–2373 (1990).
23. Rindler, M. J., Ivanov, I. E. & Sabatini, D. D. Microtubule-acting drugs lead to the nonpolarized delivery of the influenza hemagglutinin to the cell surface of polarized Madin-Darby canine kidney cells. *J. Cell Biol.* **104,** 231–241 (1987).
24. Matter, K., Bucher, K. & Hauri, H. P. Microtubule perturbation retards both the direct and the indirect apical pathway but does not affect sorting of plasma membrane proteins in intestinal epithelial cells (Caco-2). *EMBO J.* **9,** 3163–3170 (1990).
25. Lafont, F., Burkhardt, J. & Simons, K. Involvement of microtubule motors in basolateral and apical transport in kidney cells. *Nature* **372,** 801–803 (1994).
26. Hugon, J. S., Bennett, G., Pothier, P. & Ngoma, Z. Loss of microtubules and alteration of glycoprotein migration in organ cultures of mouse intestine exposed to nocodazole or colchicine. *Cell Tissue Res.* **248,** 653–662 (1987).
27. Saunders, C. & Limbird, L. E. Disruption of microtubules reveals two independent apical targeting mechanisms for G-protein-coupled receptors in polarized renal epithelial cells. *J. Biol. Chem.* **272,** 19035–19045 (1997).
28. Eilers, U., Klumperman, J. & Hauri, H. P. Nocodazole, a microtubule-active drug, interferes with apical protein delivery in cultured intestinal epithelial cells (Caco-2). *J. Cell Biol.* **108,** 13–22 (1989).
29. De Almeida, J. B. & Stow, J. L. Disruption of microtubules alters polarity of basement membrane proteoglycan secretion in epithelial cells. *Am. J. Physiol.* **261,** C691–C700 (1991).
30. Boll, W., Partin, J. S., Katz, A. I., Caplan, M. J. & Jamieson, J. D. Distinct secretory pathways for basolateral targeting of membrane and secretory proteins in polarized epithelial cells. *Proc. Natl Acad. Sci. USA* **88,** 8592–8596 (1991).
31. Grindstaff, K. *et al.* Sec6/8 Complex is recruited to cell-cell contacts and specifies transport vesicle delivery to the basal–lateral membrane in epithelial cells. *Cell Press* **93,** 731–740 (1998).
32. Lipschutz, J. H. *et al.* Exocyst is involved in cystogenesis and tubulogenesis and acts by modulating synthesis and delivery of basolateral plasma membrane and secretory proteins. *Mol. Biol. Cell* **11,** 4259–4275 (2000).
33. Low, S. H. *et al.* Differential localization of Syntaxin isoforms in polarized Madin-Darby canine kidney cells. *Mol. Biol. Cell* **7,** 2007–2018 (1996).
34. Low, S. H. *et al.* The SNARE machinery is involved in apical plasma membrane trafficking in MDCK Cells. *J. Cell Biol.* **141,** 1503–1513 (1998).
35. Lafont, F. *et al.* Raft association of SNAP receptors acting in apical trafficking in Madin-Darby canine kidney cells. *Proc. Natl Acad. Sci. USA* **96,** 3734–3738 (1999).
36. Matter, K., Hunziker, W. & Mellman, I. Basolateral sorting of LDL receptor in MDCK cells: The cytoplasmic domain contains two tyrosine-dependent targeting determinants. *Cell* **71,** 741–753 (1992).
37. Le Bivic, A. *et al.* An internal deletion in the cytoplasmic tail reverses the apical localization of human NGF receptor in transfected MDCK cells. *J. Cell Biol.* **115,** 607–618 (1991).
38. Le Gall, A. H., Powell, S. K., Yeaman, C. A. & Rodriguez-Boulan, E. The neural cell adhesion molecule expresses a tyrosine-independent basolateral sorting signal. *J. Biol. Chem.* **272,** 4559–4567 (1997).
39. Cole, N. B., Sciaky, N., Marotta, A., Song, J. & Lippincott-Schwartz, J. Golgi dispersal during microtubule disruption: regeneration of Golgi stacks at peripheral endoplasmic reticulum exit sites. *Mol. Biol. Cell* **7,** 631–50 (1996).
40. Storrie, B. *et al.* Recycling of Golgi-resident glycosyltransferases through the ER reveals a novel pathway and provides an explanation for nocodazole-induced Golgi scattering. *J. Cell Biol.* **143,** 1505–1521 (1998).
41. Wacker, I. *et al.* Microtubule-dependent transport of secretory vesicles visualized in real time with a GFP-tagged secretory protein. *J. Cell Sci.* **110,** 1453–1463 (1997).
42. Hirschberg, K. *et al.* Kinetic analysis of secretory protein traffic and characterization of Golgi to plasma membrane transport intermediates in living cells. *J. Cell Biol.* **143,** 1485–1503 (1998).
43. Rindler, M. J., Ivanov, I. E., Plesken, H., Rodriguez-Boulan, E. & Sabatini, D. D. Viral glycoproteins destined for apical or basolateral plasma membrane domains traverse the same Golgi apparatus during their intracellular transport in doubly infected Madin-Darby canine kidney cells. *J. Cell Biol.* **98,** 1304–1319 (1984).

44. Le Bivic, A., Sambuy, Y., Mostov, K. & Rodriguez-Boulan, E. Vectorial targeting of an endogenous apical membrane sialoglycoprotein and uvomorulin in MDCK cells. *J. Cell Biol.* **110,** 1533–1539 (1990).
45. Pfeiffer, S., Fuller, S. D. & Simons, K. Intracellular sorting and basolateral appearance of the G protein of vesicular stomatitis virus in Madin-Darby canine kidney cells. *J. Cell Biol.* **101,** 470–476 (1985).
46. Pfeffer, S. R. Transport-vesicle targeting: tethers before SNAREs. *Nature Cell Biol.* **1**, E17–E22 (1999).
47. Waters, M. G. & Pfeffer, S. R. Membrane tethering in intracellular transport. *Curr. Opin. Cell Biol.* **11,** 453–459 (1999).
48. Lowe, M. Membrane transport: tethers and TRAPPs. *Curr. Biol.* **10**, R407–R409 (2000).
49. Hazuka, C. D. *et al.* The Sec6/8 complex is located at neurite outgrowth and axonal synapse-assembly domains. *J. Neurosci.* **19,** 1324–1334 (1999).
50. Low, S. H. *et al.* Intracellular redirection of plasma membrane trafficking after loss of epithelial cell polarity. *Mol. Biol. Cell* **11,** 3045–3060 (2000).

ACKNOWLEDGEMENTS
This work was supported in part by a grant from the National Institutes of Health (GM34107) and by a Jules and Doris Stein professorship of the Research to Prevent Blindness Foundation (to E.R.-B.) and by an NIH National Research Service Award (EY06886, to G.K.). J.S. and S.M.S. acknowledge support from the National Science Foundation (BES0110070 and BES0119468, to S.M.S.). T.W. acknowledges support from the NIH (DK62338), the Department of Defense Prostate Cancer Research Program and the American Heart Association.
Supplementary Information accompanies the paper on www.nature.com/naturecellbiology.
Correspondence and requests for material should be addressed to E.R.B. or G.K.

COMPETING FINANCIAL INTERESTS
The authors declare that they have no competing financial interests.

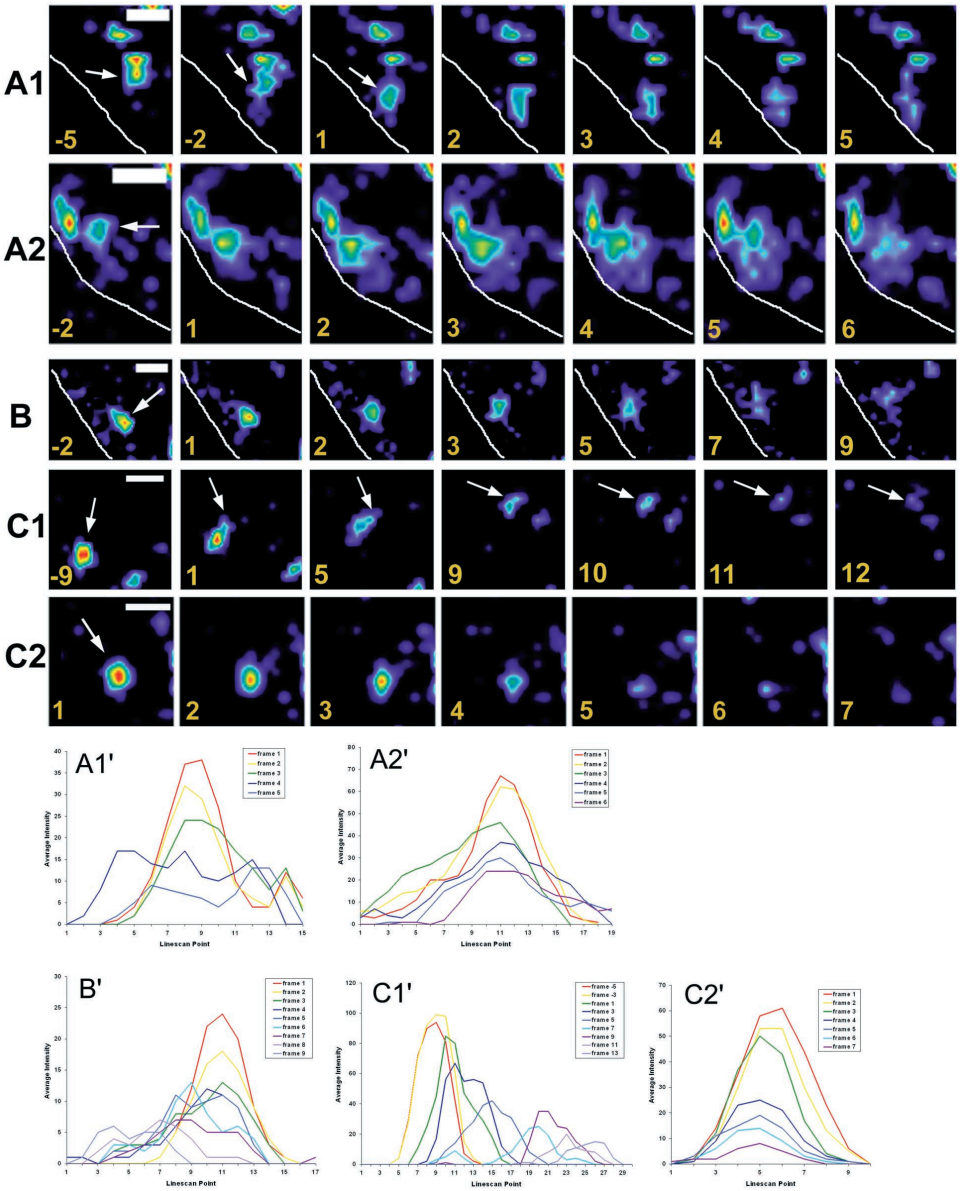

Figure S1 Behaviors of basolateral PGTIs in polarized MDCK cells. Panels in **A** and **A'** show two additional examples of PGTIs fusing with the lateral membrane. Panels in **B** and **B'** show an example of a PGTI whose fluorescence spreads primarily in one direction along the membrane over time, a characteristic suggesting either fusion with the membrane while still moving or movement in both X-Y and Z-axes without fusion. Panels in **C** and **C'** show two PGTIs near the center of the cell that move of the plane of focus. Panels in **C1** show a PGTI that moved in the XY-axis for ~2μm before prior to moving out of the focal plane in the Z-axis and disappeared. Panels in **C2** show a carrier that only moved out of the focal plane in the Z-axis. Note that while the fluorescence of the PGTIs shown in **B** and **C** moves along the XY axis, only in **B** does the width of fluorescence intensity also increase. The modest increase in the width of fluorescence intensity in **B** as compared with that in **C1** suggests that the PGTI in **B** may actually be fusing with the membrane whereas the PGTI in C definitely is not. However, since we could not unambiguously differentiate between these two profiles due to noise in our recordings, we did not ultimately classify carriers like the one shown in **B** as fusing. Lines demarcate the extracellular boundaries of the plasma membrane with the cytoplasm always to the right of the lines. Arrows denote the PGTI of interest. Frame numbers refer to the time-lapse image plane at the start of each PGTI event. Image frames were enlarged and pseudocolored for clarification. Bars = 1μm.

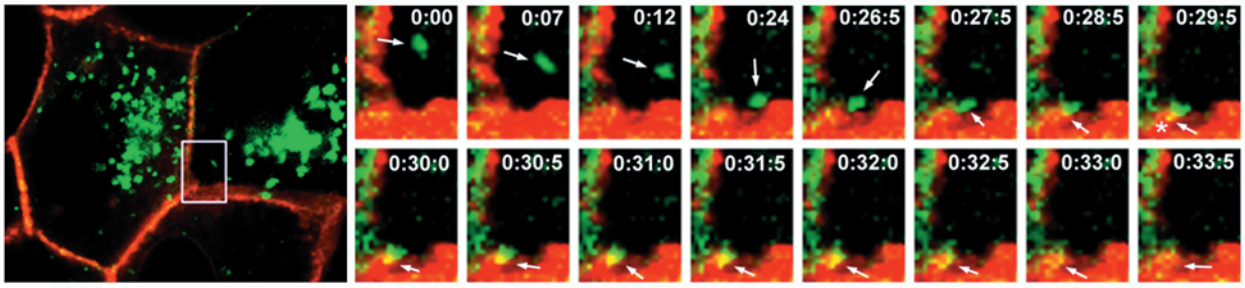

Figure S2. Fusing GFP-containing PGTIs transiently become yellow when they fuse with DiIC[16] labeled plasma membranes. Polarized MDCK cells expressing NCAM-GFP (green) were incubated with DiIC[16] (red) to fluorescently label the plasma membrane (panel A). We monitored transport and delivery of NCAM-GFP to the plasma membrane by confocal, time-lapse microscopy. Fusion of carriers with the membrane was defined by a transient change in the color of green post-Golgi carriers to yellow as they were absorbed into the red-labeled membrane. A region of one cell where a PGTI carrying NCAM-GFP clearly fused with the lateral membrane (boxed region, panel A) is shown at high magnification in selected images from a time-series (see supplemental video 1). Arrows point to a short tubular transport intermediate approaching the plasma membrane. Time stamps represent minutes:seconds:milliseconds. The asterisk in frame 0:29:5 marks the point at which the carrier first contacts the plasma membrane and begins to turn yellow. As NCAM-GFP is absorbed into the membrane, the carrier's yellow color intensifies. 3.5 seconds after the initial membrane contact (frame 0:33:0), NCAM-GFP fluorescence diffuses throughout surrounding membrane regions.

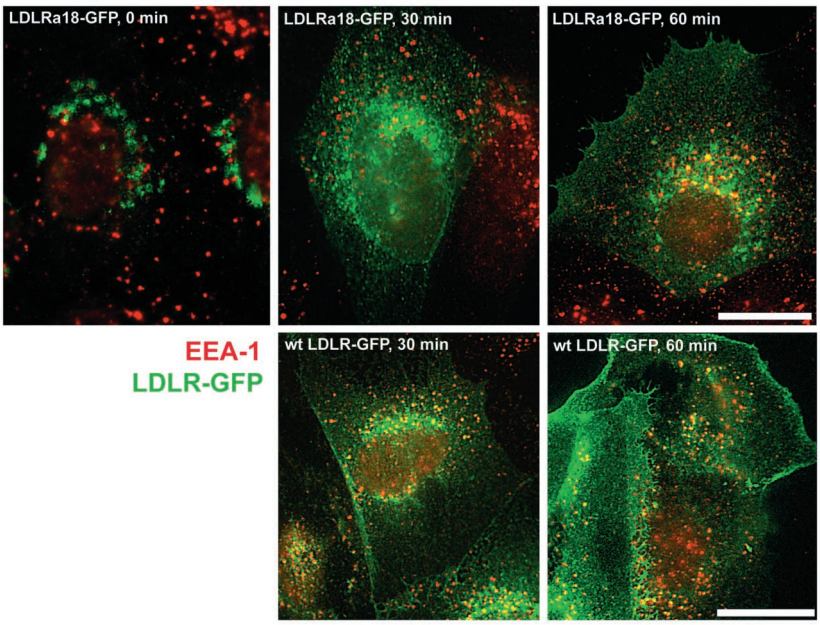

Figure S3. Recycling-defective LDLRa18-GFP does not colocalize with EEA-1 in early endosomes after release of a Golgi block. To confirm that vesicles containing LDLRa18-GFP we observed fusing with the membrane in our assays we indeed post-Golgi carriers rather than recycling endosomes, we looked for colocalization of LDLRa18-GFP with an endosomal marker. MDCK cells were injected with LDLRa18-GFP or wtLDLR-GFP, incubated at 20°C and fixed at 15 min intervals (for up to 2hr) after release of the Golgi block. Cells were immunostained with EEA1 antibody as a marker of early endosomes. wtLDLR-GFP could be detected in EEA1-positive structures as early as 30 min after release of the Golgi block indicating that it had been internalized into endosomes by this time. In contrast, LDLRa18-GFP could only be detected in a few EEA1-positive structures 60 min after release of the Golgi block.

Movie 1 Shows a single example of secretory carriers (containing p75-GFP) fusing with the basal membrane in non-polarized cells by TIR-FM.

Movie 2 Shows the spatial (Z-series) distributions of secretory carriers in polarized cells expressing p75-GFP or LDLR-GFP by confocal microscopy

Movie 3 Shows examples of fusing and non-fusing secretory carriers with the lateral membrane of polarized cells. There are two examples of fusing carriers and one example of a non-fusing carrier- I have piggy-backed the movies and inserted text frames to explain what the viewers are seeing.

Movie 4 Shows the movie in which apical carriers can be induced to fuse with the basal membrane of polarized cells when treated with nocodazole.

Movie 5 Shows the fusion of a secretory carrier with the lateral membrane using multi-color imaging and our "color-based" fusion analysis.

Methods

To confirm that fusion of carriers containing LDLR-A18–GFP we observed represented post-Golgi, rather than recycling vesicles, we analysed whether LDLR-A18–GFP carriers colocalized with EEA1, a marker of early endosomes, at various times after release of a Golgi block. Wild-type LDLR–GFP could be detected in EEA1-positive structures as early as 30 min after release of the Golgi block, indicating that it had been internalized into endosomes by this time. In contrast, LDLR-A18–GFP could only be detected in a few EEA1-positive structures 60 min after release of the Golgi block (see Supplementary Information, Fig. S3). As all our recordings of LDLR-A18–GFP were made within 60 min of releasing the Golgi temperature block, most, if not all, of the fusion events we detected probably represent trafficking of carriers from the Golgi to the plasma membrane.